LA-UR-01-4072
Approved for public release;
distribution is unlimited.

Title: **A Temperature-Based Reactive Flow Model for ANFO**

Author(s): Roberta N. Mulford and Damian C. Swift

Submitted to:

http://lib-www.lanl.gov/la-pubs/00796254.pdf

A Temperature-Based Reactive Flow Model for ANFO

Roberta N. Mulford* and Damian C. Swift
Los Alamos National Laboratory
MS E 530, Los Alamos, NM 87545, USA

Abstract

Reactive flow models for explosives are usually developed by choosing an empirical form for the reaction rate and calibrating parameters against initiation experiments. In shock wave initiation, experimental data almost always comprise mechanical measurements such as shock speed, material speed, compression, and pressure. However, we know from chemistry that reaction rates depend on temperature as well as on the mechanical state. This is one reason why mechanically based reaction rates do not extrapolate well outwith the range of states used to normalize them. For instance, mechanical reaction models which match single-shock initiation generally fail to reproduce multiple-shock initiation phenomena.

We have previously developed reactive flow models for military explosives that include temperature as well as the mechanical state. These models reproduced multiple-shock initiation behavior much more accurately than did reactive flow models with a purely mechanical reaction rate, and they were also capable of being used to simulate cook-off problems.

We have recently extended the temperature-based model for use with ANFO-type formulations. Reactive material is treated as a heterogeneous mixture of components, each of which has its own model for response to dynamic loading (equation of state, strength model, reactions.) A finite-rate equilibration model is used to determine the overall response of the mixture to dynamic loading. In the initial model of ANFO, the ammonium nitrate and the fuel oil are treated as separate components in the unreacted mixture. The ammonium nitrate reacts with a rate that depends on its thermodynamic state, with an additional contribution for brittle failure caused by shear under non-isotropic strain. The reaction products are oxygen-rich. The fuel oil decomposes or evaporates as a function of its thermodynamic state, and the decomposition products are allowed to react with the excess oxygen from the ammonium nitrate with a diffusion-limited rate which depends on the thermodynamic state. This model is also suitable for other oxidizer-fuel mixtures.

There is a relative paucity of data on initiation in ANFO formulations, so our calibrations and simulations to date are to an extent sensitivity studies of a set of equations. More experiments are needed before the model can be regarded as accurate for predictive work.

Improved models are under development, in which we intend to incorporate enough flexibility to reproduce experimentally observed shock desensitisation while retaining plausible and computationally practical physical models for the equations of state (unreacted, partially-reacted and products), equilibration processes and reaction rate.

*mulford@lanl.gov

LA-UR-01-4072
Approved for public release;
distribution is unlimited.

Title: **A Temperature-Based Reactive Flow Model for ANFO**

Author(s): Roberta N. Mulford and Damian C. Swift

Submitted to:

http://lib-www.lanl.gov/la-pubs/00796254.pdf

Contents

1 Introduction

The detonation of ammonium nitrate / fuel oil (ANFO) explosive provides a demanding challenge to hydrocode modelling, as the multiple processes involved in the decomposition and reaction, coupled with the relatively long reaction zone compared to the charge size in many applications, make the performance of the explosive highly non-ideal [1]. Furthermore, ANFO-type explosives are used with a wide variations in composition, particle size and porosity, making it desirable to be able to predict the initiation and performance properties without having to re-calibrate the reactive flow model for each variant.

The objective of this work was to develop models capable of predicting the initiation and blast behaviour, and capable of treating variations in composition and morphology, and different loading conditions. We found previously [2, 3] that it was important to use a reactive flow model which is based on sound physical processes in order to achieve a reasonable predictive capability. We describe here the structure and calibration of a model which represents the actual physical structure of ANFO explosive in simplified form, and which uses temperature-dependent reaction rates.

Because chemical kinetics is governed primarily by temperature, we have attempted to model detonation as a function of temperature, rather than just pressure. Previous application of this model to military explosives [2, 3] indicated that this type of reaction model can adequately describe initiation of these explosives, accurately modelling both chemical terms and heating due to porosity ("hotspot" terms.) This type of model should be particularly valuable in simulating the behavior of non-ideal explosives such as AN, where the chemical reaction is not prompt at the pressures studied.

The value of the work presented here lies in addressing chemical processes directly, thereby enabling chemical kinetic data reported in terms of temperature (and at STP, generally) to be used in shock reaction models. Kinetic data expressed in terms of P, though more directly applicable to the case at hand, are rare.

Fundamental data and physically-based models are of particular value in evaluating candidate methods for desensitising a mixture by altering its composition, as these may typically involve a wide range of materials and states. Physical and performance data may be scarce for some of these systems. However, chemical reactivity data such as rates, activation energies, and heats of reaction may be readily available or easily estimated.

Models developed with consideration for the underlying physical processes occurring in an explosive are far more likely to be applicable to new situations - and hence provide a predictive capability - than are empirical models calibrated against a restricted set of experimental data.

2 Physical processes and chemical reactions

At some level of treatment, thermal terms govern the chemical kinetics in any explosive. Our previous studies have shown that temperature-based reaction rates can be used reliably, if heterogeneities are taken into account in an adequate way. [2, 3] The resulting reactive flow models should have a better predictive capability than simpler empirical models. This makes them valuable for formulations such as AN and oxidizer-fuel mixtures where the composition, morphology, and porosity can vary widely.

In non-ideal explosives such as AN, the chemical reactions may not be prompt or simple, and consequently the observed behavior of the system may be governed not by reaction in response to pressure at the wave front, but by a reaction of chemical components which is slow relative to shock processes. The reaction rate may be governed by the slow mixture or reaction of products from two or more components, or by delayed reactions; multi-step reactions in which energy is evolved in late steps.

The mechanism that we expect for AN proceeds roughly by the following steps. Upon shocking the AN is heated by the passage of the shock. This heating arises from deformation of the bulk solid, from compression of gas in the pores in the material, and from plastic flow or brittle fracture in the solid. Once heated by some mechanism, the ammonium nitrate reacts with a temperature-dependent rate, heating itself, the fuel oil and the products. The hot fuel oil reacts with the oxygen-rich products of the AN decomposition, in a reaction which may be modelled in one of four ways. The fuel oil may evaporate, and the vapor react in the gas phase with the product gases from AN. The fuel oil may undergo thermal decomposition to products, which react in the gas phase with the product gases from the AN. We neglect this pathway, as less likely than the first, and thermodynamically very similar to it. The fuel oil may react with the product gases by surface-burning. This mechanism differs thermodynamically from the first mechanism by the heat of evaporation of the fuel

oil, and produces a different rate of reaction between the fuel oil and the AN products. Finally, oxygen-rich species could diffuse into the fuel oil and react *in situ*. We neglect this pathway as condensed fuel oil is less likely to react than is the vapour, and the diffusion rate for molecules of fuel oil or its decomposition products is likely to be higher in the hot products than *vice versa*.

Grain size governs porosity and pore-size, and consequently affects reaction, by increasing the density of potential hotspots, while reducing their size. Smaller voids are recognized to be ineffective in producing reaction because rate-dependent strength makes smaller voids more difficult to compress, and because the greater surface area to volume ratio of small hotspots permits them to cool faster. We use thermal diffusion as a measure of grain size within the model.

As with other explosives, the porosity of the AN has been observed experimentally to make a difference in its reactive behavior. Several mechanisms may contribute to enhanced reaction of the AN at pores. P-V heating is the most obvious term, but our previous work indicates [3] that neither bulk heating alone, nor a model with enhanced reaction in the heated zone around a collapsed pore is sufficient to mimic observed reaction rates in HMX-based explosives. Other mechanisms that may be active are plastic work or else brittle fracture in the material around the pore. Plastic work appears to be an important heating mechanism in military explosives. [2, 8] A model based on plastic work has been developed for AN. [5] Brittle fracture is possible given the ceramic nature of AN, and might contribute to the heating[6]. The importance of viscosity and resulting energy delocalization in hotspot behavior has been discussed. [2]

Because many material properties include flow stress, viscosity and thermal conductivity depend on temperature, and hotspot mechanisms as well as chemical reaction rates are somewhat dependent on bulk temperature. [2]

A term for plastic work should ideally be included in a model of this type. While some effort has gone into treating this term, plastic work at pores is not currently included in this model [1].

Shear bands that form in response to the shock are a mechanism for localization of the mechanical energy of the shock. Localization of energy on lattice defects will behave similarly. Formation of shear bands is greatest when the material, or a component, such as AN, is brittle.

3 Reactive flow model

We developed a continuum-level model to represent the known or suspected physical processes in as realistic a way as is commensurate with our understanding of the mechanical behavior and chemistry at the microstructural level. Physically based models can be expected to have a greater region of validity, and it is often possible to calibrate them against accurate static measurements, rather than varying parameters to match a dynamic simulation to an integrated experiment.

Ideally a reactive flow model should treat chemical processes with fidelity to the rates and energy releases expected for the system, sufficient to determine the rate-governing step under different stimuli. The model should describe the mechanical properties for each spatially distinct phase in the composition, including the equation of state (EOS) and elastic-plastic behaviour, with a description of the evolution of the population of dislocations. The local state in each computational cell might describe the spatial distribution of each component of the composition, and the distribution of the thermo-mechanical state (density, temperature, elastic strain, dislocation density) in each phase. The use of some form of distribution might be used to represent the variation in particle size and in the temperature in bulk material near a hotspot. Each distribution might be a quantised population (e.g. considering the evolution of particles of a range of discrete sizes) or some smooth representation.

Currently, such a model would require materials property data that are not available, and the amount of data required to describe a dynamically deforming system would use a prohibitive amount of storage and computational time.

The model used here attempts to provide enough freedom to model the initiation and reactive behavior of many explosives, while still running in a reasonable time. The models at least addresses microstructural processes, without treating them fully. Initial values for most parameters were obtained from the composition, heats of formation, and other measured properties of the unreacted explosive, rather than by calibration against dynamic experiments. Microstructural processes are represented in a way which should be 'forward

[1] Plastic flow has subsequently been incorporated and used to model HMX-based explosives [9]

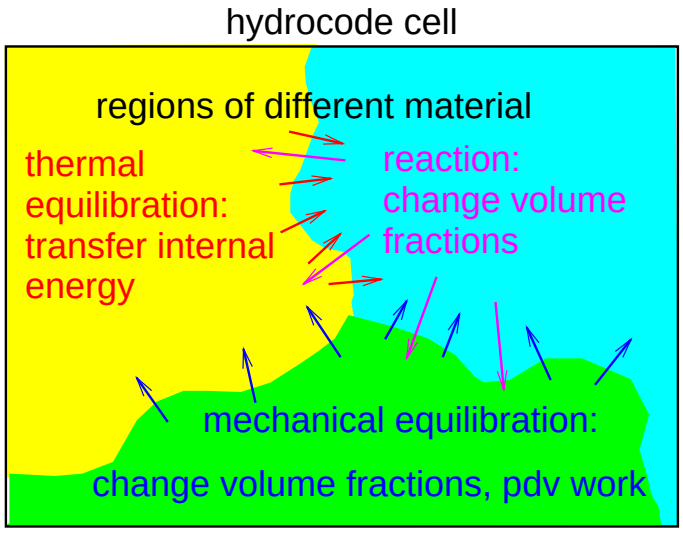

Figure 1: Schematic of the heterogeneous model.

compatible' with detailed simulations of the microstructural behaviour, i.e. we intend in the future to use the results of mesoscale simulations to calibrate our simplified model of the microstructural behaviour.

Since the model was designed for use in continuum mechanics, it consists of a local state (varying with location and time inside a material subjected to dynamic loading) and a description of the material response (the same throughout a particular material). The material response model uses the local state to calculate 'external' properties such as mass density, stress and temperature, and to calculate the evolution of the state given applied loading and heating conditions. For an unreactive material, the simplest such model uses the density and energy to define the local state, and the EOS as the response model. For reactive materials, our local state comprises the internal state and volume fraction for each spatially distinct region in the microstructure. This is therefore a heterogeneous mixture model. The material response model includes the model for each component of the heterogeneous mixture, and a set of reaction rates. The reaction rates are used to transfer material between components, and also to describe reaction within a component if appropriate. The state and material response in each component depends on the material type used: it may be a traditional EOS, a thermodynamically complete EOS taking density and temperature as its local state, a constitutive model including strength or viscosity, or a homogeneous mixture of chemical components.

Since each component has its own state, a pressure and temperature can be calculated for each. Pressure and temperature are equilibrated explicitly according to a separate time constant for each. This produces an exponential approach to mechanical and thermal equilibrium separately. Ideal equilibration can be enforced by setting the time constants to a small value. Pressure equilibration was performed by adjusting the volume fraction of each component towards equilibrium, and expanding or compressing along an isentrope. Temperature equilibration was performed by transferring heat energy at constant volume. The time scales were estimated from the grain size and properties of each component. In principle, they could be considered as additional continuum variables and evolved according to other microstructural processes.

Porous materials were represented by starting with a non-zero volume fraction of products. This model is not appropriate for all circumstances, but it was found to be reasonable for pores containing low density gas such as air.

An Arrhenius rate law was used, as probably the most physical representation of the chemical reaction process at the molecular level. 'Bulk' and 'surface' reactions were included, using the same reaction rate, but with the temperature of the adjacent component in the surface reaction. If the surface reaction rate was significant, material was burnt using a flame propagation model. The surface term included a description of the contact area between pairs of components in the heterogeneous mixture, estimated from the initial grain sizes and the volume fractions present at any stage in the reaction.

This model is fairly general and flexible. It can be used to describe simple single-parameter reactive flow,

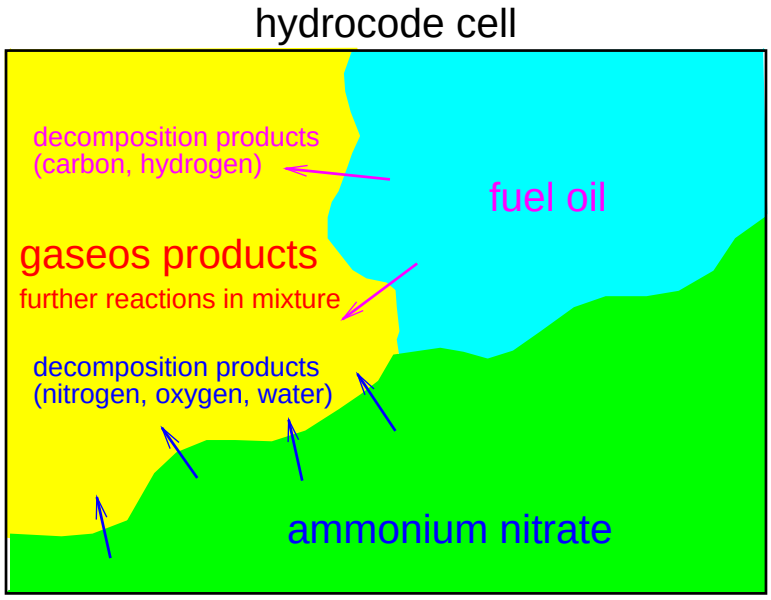

Figure 2: Schematic of the model for ANFO.

such as the Lee-Tarver model, as a special case.

For ANFO itself, the heterogeneous components considered were AN, fuel oil, and gaseous products. AN and fuel oil were described by thermodynamically complete EOS, discussed later. The products were represented by a chemical mixture model allowing a variation in composition. The chemical components in the products included a simplified set of AN products (N_2, H_2O and O_2), fuel oil, and a simplified set of ANFO reaction products (CO_2) in addition to the AN products. The inclusion of this set of molecules allows us to treat effects of composition such as oxygen balance with no adjustments except to change the volume fraction of each component in the virgin material. We could have included a model for the decomposition of the fuel; in the case of fuel oil it is more likely that the oil would evaporate and burn on mixing with the AN products. The decomposition of AN was modelled by an Arrhenius rate law, transferring material to the products region. Evaporation of the fuel oil was represented by the surface reaction scheme, Reaction between AN products and decomposed fuel oil were modelled by an additional Arrhenius law, altering the composition and temperature in the products.

The initial porosity was treated explicitly using the mixture model, by including a heterogeneous component comprising pore gas. The pore gas could be modelled using its actual EOS, for instance air. For reactive mixtures it is computationally more efficient to model pore gas as an initial fraction of reaction products since there is then one component fewer in the calculations and it is in any case likely that gaseous components will become intimately mixed. We found previously [3] that detonation products – for which a plausible STP state can usually be found – actually represent air with adequate accuracy. Pore collapse gave increased heating and thus increased the reaction rate through the surface terms. (Fig. 2.)

A Lagrangian hydrocode was used to simulate dynamic experiments and hence allow the models to be evaluated against experimental data. The hydrocode used a finite difference representation of the continuum equations, integrating the hydrodynamics with a predictor-corrector scheme. Shock waves were stabilised with Wilkins' bulk artificial viscosity. Reaction was operator-split from the hydrodynamics and subcycled, using a forward-time integration scheme. Equilibration of pressure, temperature equilibration and chemical reactions were operator-split from each other and subcycled.

4 Equations of state for condensed phases

Temperatures should be reasonably accurate in order to use a temperature-dependent reaction rate. A reliable value of heat capacity at STP permits an estimate to be made, but heat capacity depends on temperature and density. Temperature dependence arises from population of modes available for absorbing thermal energy: phonons in solids and vibrations in molecules. A careful treatment of the population of these modes as a function of the energy of the mode was made, in order to provide an EOS which included a temperature.

The equation of state for condensed phases was quasiharmonic, consisting of a cold curve (or $T = 0$ isotherm) and a set of non-interacting modes corresponding to vibrational, rotational and translational degrees of freedom. The cold curve was defined in terms of the variation of specific internal energy e_c with mass density ρ. Given $e_c(\rho)$, the cold curve pressure p_c can be found readily from

$$p_c(\rho) = -de_c/dv \tag{1}$$

where v is the specific volume, $1/\rho$. A set of vibrational modes $\{\omega_i(\rho)\}$ was considered. Given the cold curve and the $\{\omega_i\}$, the specific internal energy can be found for all states from

$$e(\rho, T) = e_c(\rho) + \frac{1}{m}\sum_i \hbar\omega_i(\rho)\left\{[\exp(-\hbar\omega_i(\rho)/k_BT) - 1]^{-1} + \frac{1}{2}\right\}, \tag{2}$$

which is the energy of a set of oscillators with Bose-Einstein statistics. Similarly, the pressure can be found from

$$p(\rho, T) = p_c(\rho) - \frac{1}{m}\sum_i \hbar\frac{d\omega_i}{dv}\left\{[\exp(-\hbar\omega_i(\rho)/k_BT) - 1]^{-1} + \frac{1}{2}\right\}. \tag{3}$$

For the present work, these functions were computed in-line during reactive flow simulations. They may also be tabulated in the manner of the SESAME tables [28]; this is more efficient for repeated or large-scale simulations. The equations of state were used in an explicit (ρ, T) form in the reactive flow program: the state in these materials was represented by its density and temperature rather than density and internal energy. As mechanical work or heat was applied to an element of material, the temperature was allowed to evolve according to the appropriate value of its specific heat capacity, $c_v = \partial e/\partial T|_v$, calculated from the expression for $e(\rho, T)$ above. A predictor-corrector scheme was used for second-order accuracy, and the scheme was subcycled with a specified limit on temperature change in each cycle.

Ideally, the quasiharmonic equation of state would be calibrated using a cold curve and a set of frequencies (including their individual variations with compression), obtained from a rigorous theoretical model or direct experimental measurements. Unfortunately, neither set of data was available for the condensed components of ANFO. Instead, the cold curve was estimated from the shock Hugoniot, and the vibrational modes were obtained from the literature [19, 20] or estimated by considering from structure of each type of molecule and frequencies measured for similar molecules.[20]

The cold curve was inferred by using a mechanical equation of state fitted to measured states on the shock Hugoniot, and assuming a simple model for off-Hugoniot states. A value was assumed for the density at $T = 0$, the specific internal energy necessary to give $p = 0$ was found from the mechanical equation of state, and the equation of state was integrated at constant entropy to estimate $e_c(\rho)$. This method has been applied previously to nitromethane, and performed well with a simpler model of vibrational modes [4]. The Steinberg form [11] of Grüneisen equation of state was chosen for its computational convenience. The primitive experimental data used were measurements of the speed u_s of a shock wave in the sample material as a function of the material (or particle) speed u_p. In the Steinberg form of Grüneisen equation of state, this relation is represented by the functional form

$$u_s = c_0 + \sum_{i=1}^{n} s_i \left(\frac{u_p}{u_s}\right)^{i-1} u_p, \tag{4}$$

where c_0 and the s_i are fitting parameters, and the summation is usually extended to $n = 3$ for a cubic Grüneisen form. This equation is non-linear in u_s and u_p, but apart from c_0 the coefficients are dimensionless, so it is straightforward to choose different sets of units.

In addition to the $u_s - u_p$ fit, the Grüneisen equation of state comprises the initial mass density ρ_0 and specific internal energy e_0, and the variation of the Grüneisen parameter Γ with compression. ρ_0 is usually measured before performing a shock wave experiment; $e_0 = 0$ at STP by convention. Ideally, Γ is determined as a function of ρ by further experimental measurement, such as the variation of sound speed with compression in a succession of shocked states. However, Γ can also be estimated from the gradient of the $u_s - u_p$ relation, and for a material with a cubic crystal structure and a linear $u_s - u_p$ relation it is accurate to take [10]

$$\Gamma = 2s_1 - 1. \tag{5}$$

It can be seen that Γ is constant for a linear Grüneisen form ($n = 1$), but that Γ varies with compression for $n > 1$.

Where a linear $u_s - u_p$ fit had been published (as was the case for for ammonium nitrate), it could be used to obtain c_0 and s_1 directly. Where the original shock wave data was available (as was the case for fuel oil), the equation of state was calibrated against the data using a fitting procedure described elsewhere [12].

Given this mechanical equation of state and an estimate of ρ at $T = p = 0$, the corresponding energy could be found, and hence the cold curve by integrating $p\,dv$ work from that state. Over a range of several tens of GPa, it was found that the difference between the Hugoniot and the cold curve was much larger than the sensitivity of the cold curve to the precise choice of initial density.

For the molecules of interest, no data was found on the vibrational modes $\{\omega_i\}$ or their variation under compression. Values of $\{\omega_i\}$ were estimated at STP from the structure of each molecule. The accuracy of the modes was evaluated by comparing with the measured heat capacity at STP, or its variation with temperature. The variation with compression was estimated by assuming that $\gamma_i = (v/\omega_i)d\omega_i/dv$ was constant for each mode, and equal for all modes. The value of this logarithmic derivative was calculated by finding the unique value which, when the corresponding quasiharmonic modes were added to the cold curve, reproduced the original STP state. The form assumed for the γ_i implies that the frequencies vary as

$$\omega_i(v) = \alpha \exp(-\gamma_i v/v_0). \tag{6}$$

This is arguably a better-justified form than the linear variation with density which has been used for nitromethane [29] and is presumably valid over a smaller range of compressions; however it is unlikely that all frequencies would have the same value of γ_i in reality.

5 Equations of state for ammonium nitrate

Hugoniot data for AN is available from a variety of sources [15]. The data of Courchinoux and Lalle was selected and used in a Steinberg-style Grüneisen EOS. The EOS parameters were c_0=1.8 km/s, s_1=1.8, and Grüneisen's $\Gamma = 2.6$.

The cold curve was obtained from the fit by estimating the density at $T = 0, p = 0$, deducing the energy from the Steinberg equation of state, and integrating the equation of state isentropically up and down in compression. However, the fitting procedure is more complicated.

The STP density for solid AN was taken to be 1.728 g/cm^3 – a median value from the data. A compression of 2.5% was assumed between STP and 0 K, giving a density of 1.7712 g/cm^3. Compared with the Hugoniot, the cold curve did not depend very sensitively on the density assumed at 0 K. (Fig. 3.)

5.1 Vibrational frequencies

The 21 vibrational frequencies of ammonium nitrate are estimated from the frequencies of ammonium ion [19], the frequencies of nitrate ion, [19] nitric acid $HONO_2$, and salts $FONO_2$ and $ClONO_2$. [20] The only frequency diverging appreciably from the template spectra is that of the N-O stretch between the ammonium and nitro groups. This type of N-O stretch can assume any value between about 1000 and about 3000 cm^{-1}, and is placed at 900 cm^{-1}, by analogy with the F-O bond in $FONO_2$, since the mass of the fluorine atom approximates the mass of the ammonia ion.

The change in frequency as a function of pressure can be expected to be slightly different for each vibrational mode [36]. None of these sensitivities could be determined explicitly, in the absence of high pressure vibrational spectra. Instead, we assumed a single constant value for the logarithmic derivative of

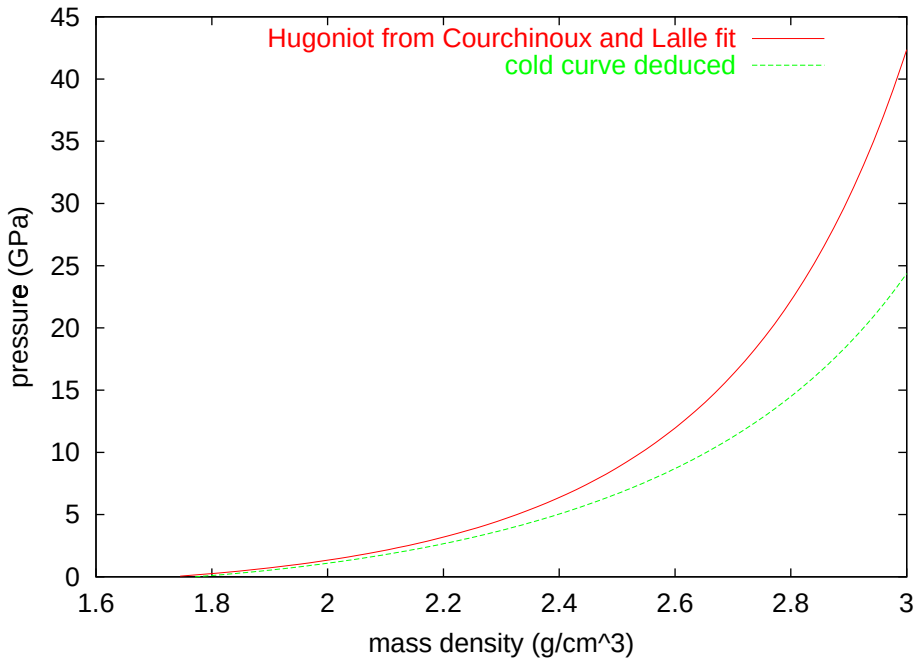

Figure 3: AN: density – pressure curves.

Table 1: Vibrational modes for ammonium nitrate

mode	wavenumber (cm^{-1})	degeneracy (modes per molecule)
O-H bending	1300	2
O-H stretching	3700	1
NH_3 umbrella	1400	3
NH_3 stretch (as)	3145	3
NH_3 scissor	1680	2
NH_3 stretch (s)	3040	1
O-NH_3 torsion	150	1
O-NO_2 i.p. bend	710	1
O-NH_3 bending	300	1
N-O bending	450	1
N-O bending	630	1
NO_2 scissor	800	1
O-NH_3 stretching	900	1
NO_2 stretch (s)	1300	1
NO_2 stretch (as)	1760	1

Rotations and translations of the whole molecule are not included in the table.

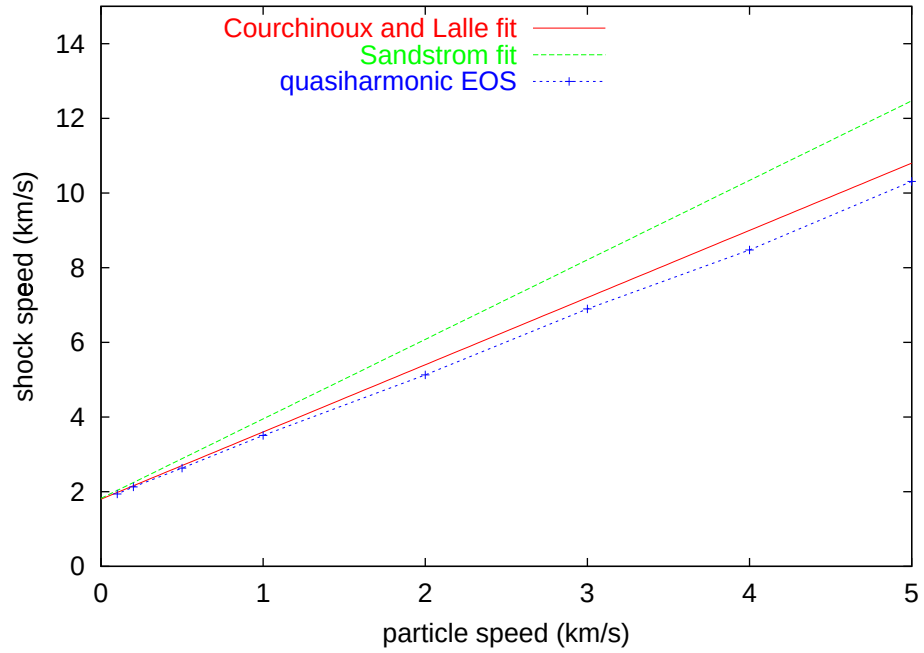

Figure 4: AN: Hugoniots.

all the frequencies and determined it by iteration to reproduce the STP state. The value obtained in this way was $(v/\omega_i)d\omega_i/dv = 0.028721326$.

We assumed that the frequencies corresponding to translational and rotational modes of the molecule in the solid were negligible compared with the molecular modes, and associated a heat capacity of k_B per mode for each to allow for kinetic and potential contributions.

The vibrations were combined with the cold curve as discussed above to obtain a thermodynamically complete EOS.

Using the vibrational frequencies, the specific heat capacity at constant volume c_v for the STP state was predicted to be 1071.59 J/kg.K. The observed heat capacity at constant pressure c_p is 1740 MJ/kg.K [23]. c_p is generally greater than c_v, by an amount k_B per molecule for a perfect gas [7]. The difference here is somewhat greater than might be expected for a solid. It is unlikely that electronic excitations contribute significantly to c_v at STP. Almost all of the molecular modes are quenched – they are predicted to contribute only about 1.46 k_B per molecule at STP – so frequencies significantly lower than the estimates could increase c_v. However, it is unlikely that the frequencies are much in error, so we suggest that the difference is largely real and reflects the non-classical behaviour of hydrogen-rich molecules.

The Hugoniot obtained from the quasiharmonic EOS reproduced the Grüneisen fit reasonably well; certainly within the range of experimental Hugoniots obtained by different workers [15]. (Fig. 4.)

5.2 Porous AN

As discussed above, initial porosity can be treated explicitly using the mixture model. A significant advantage for continuum simulations is that no further adjustments are needed to predict the effect of changes in porosity, beyond choosing the initial volume fraction for the pore gas. The evolution of porosity under different loading histories (e.g. multiple shocks) is also handled seamlessly. This approach is significantly more convenient than applying empirical adjustments to the Hugoniot [32, 33, 34], and it appears to be at least as accurate.

Predictions were made of the porous Hugoniot for AN by performing hydrocode simulations of shock propagation in the porous material with different piston velocities applied at one end, and using air (repre-

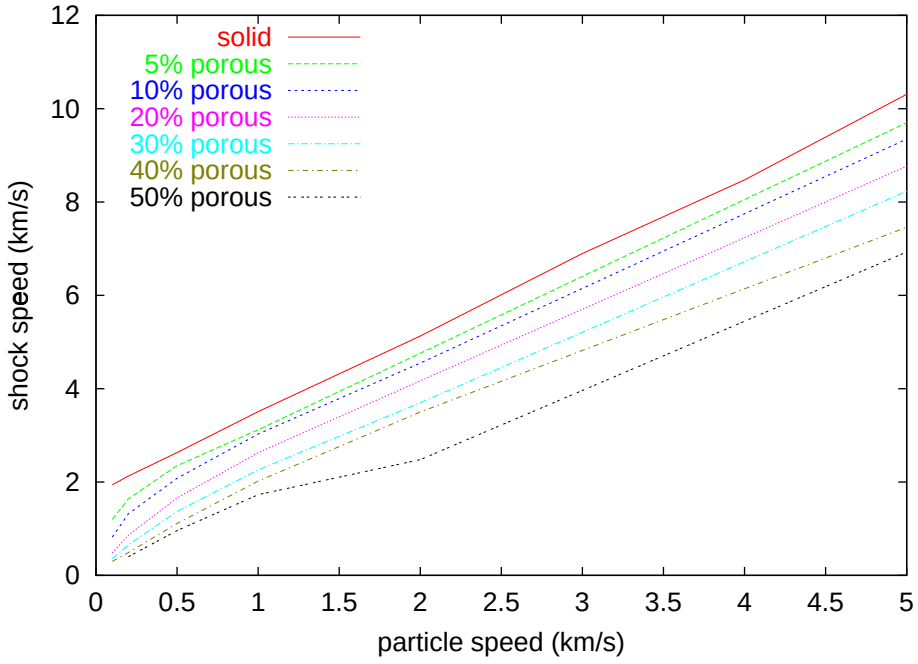

Figure 5: AN: porous Hugoniots predicted using quasiharmonic EOS and ideal equilibration (infinitesimal particle size).

sented by a perfect gas EOS) as the pore gas. Shock speeds were determined using the artificial viscosity q from the position of the maximum in q/ρ as a function of time. At higher porosities and lower pressures the shock broadened into a gradual compaction which took some time to become steady. There was thus some uncertainty in the velocity (probably responsible for the kink at 50%) though as consistent a method as possible was used. (Fig. 5.)

The heterogeneous mixture method described here accurately modelled subtle details of the porosity-dependent initiation behavior of HMX-based military explosives, where the porosity was ∼1% or less [2, 3]. In AN, numerical problems occurred in the previous two-component mixture model for porosities above about 15%, apparently caused by regions of state space in which the sound speed became imaginary. The problems could be ameliorated but not removed by adjusting the equations of state of the product gases. The new multi-component mixture model included more accurate equilibration schemes (second order predictor-corrector rather than first order forward difference, with adjustments to conserve energy to a high accuracy [35]), and the model was found to operate with porosities up to at least 50%.

Ideally, we would like to calibrate models of mechanical response and reaction by comparing with data from 1D shock wave experiments. Shocks which are (initially) constant in space and time – i.e. planar and well-supported – make it much easier to interpret and model of the data. Suitable data exist for the Hugoniot of 45% porous AN [32]. In these experiments, shocks were generated by the direct impact of an explosively-driven flyer plate accelerated in a mousetrap configuration. The article velocity u_p, was measured directly at several Lagrangian positions, using electromagnetic velocity gauges [37]. The shock velocity u_s was obtained from the time of arrival at the different gauges. A stirrup gauge on the explosive surface recorded the profile of the input wave generated at impact. In one of the experiments the shock speed was anomalously large, which was attributed to reaction. This point was disregarded when comparing to the unreactive porous models, but was used subsequently as an experimental run distance for shock initiation.

The quasiharmonic EOS gave a reasonable fit to the experimental data, somewhat worse at higher pressures. The calculated Hugoniot was not sensitive to the equilibration rates or mesh size, and was unchanged on using a SESAME EOS for the pore gas instead of the perfect gas EOS. Excellent agreement could be obtained by using the Steinberg EOS more directly, with a cold curve and constant heat capacity

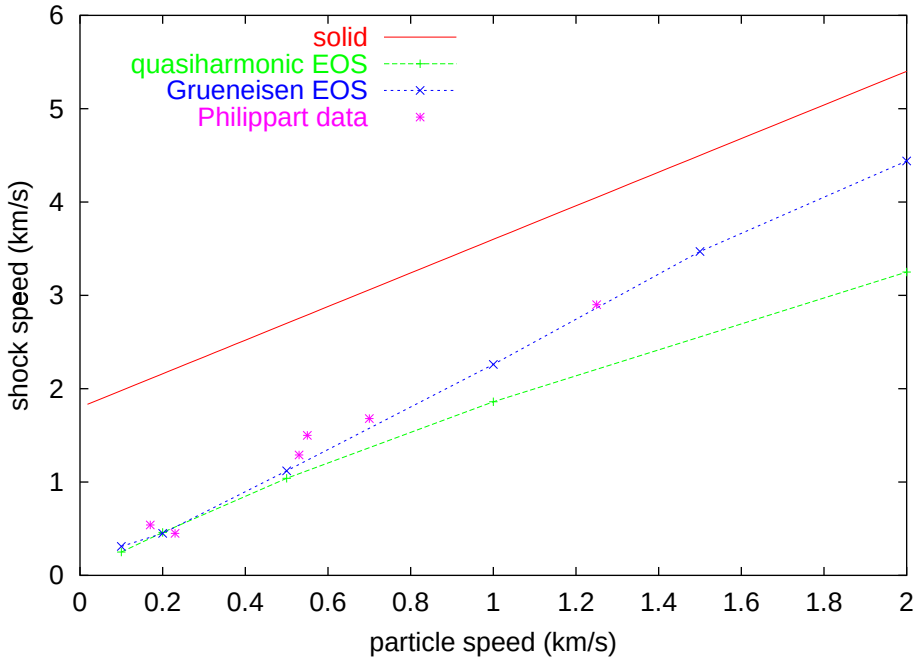

Figure 6: AN: Hugoniot at 45% porosity.

to provide an estimate of the temperature. The difference between the quasiharmonic EOS and the data is thus likely to reflect the deviation between the quasiharmonic EOS and the $u_s - u_p$ fit. We prefer the quasiharmonic EOS for simulations of reactive flow because the temperatures are much more likely to be accurate. (Fig. 6.)

6 Equation of state for fuel oil

The equation of state for fuel oil (FO) was obtained by the same method used for AN. No compression data was found for fuel oil, so we assumed that the properties would be similar to those of paraffin, for which Hugoniot data have been published [13]. Steinberg's form of Grüneisen EOS was fitted to the data as discussed above. In contrast with the published fits for AN, non-linear terms were needed to represent the data on paraffin.

The Hugoniot was fitted with a cubic Grüneisen form, with parameters c_0=1.8034km/s, s_1=3.56525, s_2=-5.2109, and s_3=2.82867. Grüneisen's Γ was taken to be constant, 2.04846. (Fig. 7.)

The density at STP, $\rho_0 = 0.9185\,\mathrm{g/cm^3}$. The density at $T = 0, p = 0$ (ρ_0^0) was estimated to be $0.964425\,\mathrm{g/cm^3}$, a 5% decrease from the STP value. (Fig. 8.)

6.1 Vibrational frequencies

As with AN, molecular vibrations were used to modify the cold curve, to produce a Hugoniot at finite temperatures.

Fuel oil is approximated by saturated single chain olefins C_nH_{2n+2}, where n may vary. For n carbons, we expect $3n - 6 = 9n$ vibrational modes. In order to determine a generic spectrum, the infrared spectra of various structural isomers of C_4H_{10} and C_6H_{14} were compared. [22] In molecules such as hexane, the exact configuration (cis- or trans- at each C-C bond) determines the frequencies, to within about 30 to 50 $\mathrm{cm^{-1}}$. As a variety of configurations can be anticipated, the frequencies were grouped into bands of between 40 $\mathrm{cm^{-1}}$ and 100 $\mathrm{cm^{-1}}$ in width, on the assumption that the large number of configurations present will provide an average approximately equal to the center of the band, the frequency used. The larger the

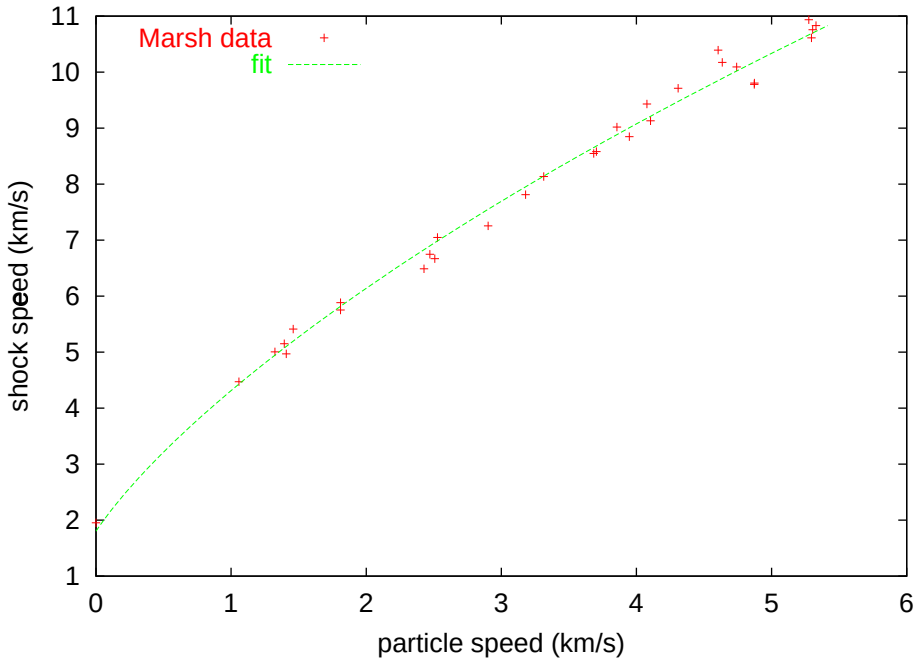

Figure 7: Steinberg fit to paraffin Hugoniot.

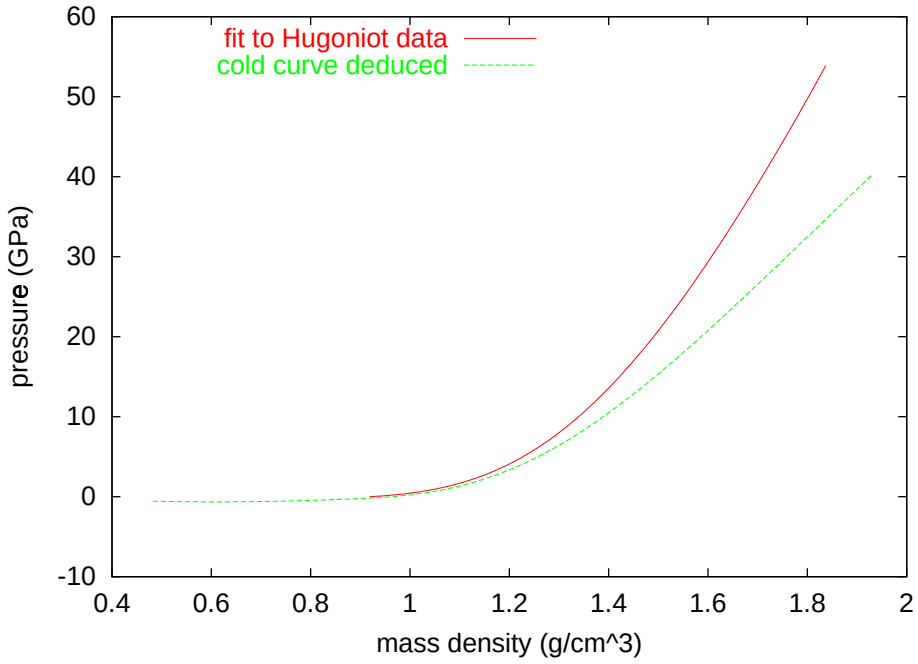

Figure 8: Density – pressure curves for paraffin.

Table 2: Vibrational modes for C_nH_{2n+2} molecule, "fuel oil"

predominant mode	wavenumber (cm^{-1})	width ($\pm$ cm^{-1})	degeneracy (modes / molec)
torsion	200	100	$n-1$
skeletal bends	400	100	$n-1$
CH_2 rock	760	40	$n/2$
CH_3 rock	900	50	$n-2$
C-C stretches	1050	40	$n-2$
CH_3 rock	1140	10	2
CH_2 twist	1250	30	$n/2$
CH_2 wag	1350	10	n
CH_2 scissor	1450	30	$n+2$
CH stretches	2900	50	$2n+2$

Rotations and translations of the whole molecule are not included in the table.

molecule, the more normal modes may be expected, and accordingly, the number of frequencies falling within each band is expressed in terms of the chain length, n. Where the number of frequencies cannot in practise be determined from a knowledge of the molecular vibration principally responsible for the frequencies, e.g. hydrogen stretching modes or carbon skeletal bends, the number of frequencies is estimated by comparison of a number of spectra of different molecules. [22]

The change in frequency as a function of pressure was described, in the absence of high pressure vibrational spectra, by a single value for all modes. This was estimated as the value necessary to reproduce the STP state, $(v/\omega_i)d\omega_i/dv = 0.035476$.

The Hugoniot produced from the quasiharmonic equation of state was a reasonable fit to the Marsh data up to about 20 GPa. At higher pressures, the calculated Hugoniot fell below the data. As with AN, there are several possible explanations: the cold curve calculated using the Grüneisen model may be too soft; the vibrational frequencies may increase too slowly with compression in this region; or the quasiharmonic assumption may break down as compression or temperature increase because of mixing of the modes, caused by the large number of modes and the small energy differences between them. (Fig. 9.)

7 Simplified chemistry

To determine the products to be used in the model, balanced chemical equations were used, producing products which maximized the enthalpy of reaction. No adjustment for the temperature of the reaction was made. Observation of the products from a typical AN reaction indicates that a certain amount of soot is produced, and probably some nitrogen oxides. [25] These and other products of incomplete reaction are probably preserved by the dispersion of products on a timescale faster than reaction. However, for the present model, the products selected were satisfactory.

Products to which AN can react in isolation were considered. Of the possible products H_2, O_2, N_2, H_2O, NH_3, NO, HNO, and NO_2, only the reaction to N_2, H_2O, and O_2 is thermodynamically favorable at STP:

$$NH_4NO_3 \rightarrow N_2 + 2H_2O + \frac{1}{2}O_2 \qquad \text{Enthalpy of reaction} = \text{-28.2 kcal/mole of AN.} \tag{7}$$

Other species may of course be produced during reaction at elevated temperature and pressure, and these may persist if the products expand and cool more rapidly than further reaction to the thermodynamically favorable products can occur. However, in the present work we restricted ourselves to the ideal products only.

The oxidiser/fuel reaction was modeled using three separate processes. The AN oxidiser decomposes leaving oxygen-rich products as discussed above; the fuel vaporises as it is heated by compression and conduction; excess oxygen from the AN reacts with the vaporised fuel.

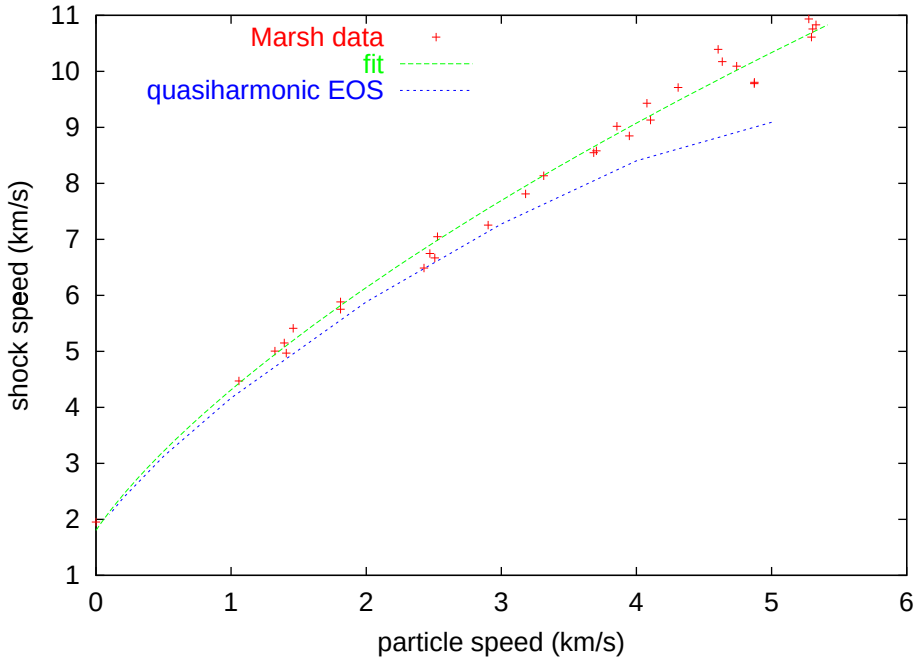

Figure 9: Hugoniots for paraffin.

The fuel oil was taken to be an olefin, composition C_nH_{2n+2}, with a molecular weight of $14n + 2$. The chain length n is almost immaterial, but it provides a mechanism for counting atoms. We used $n = 10$ for convenience. As with the decomposition of AN, we considered only the reaction which produced the thermodynamically favored products at STP:

$$C_nH_{2n+2} + \frac{3n+1}{2}O_2 \rightarrow nCO_2 + (n+1)H_2O \qquad \text{Enthalpy of reaction} = \text{-1564 kcal/mole of paraffin.} \quad (8)$$

8 Equations of state for reaction products

The products consist of a number of gaseous chemical species. The concentration of each specie may vary during the course of the simulation as the gaseous species react with each other. We would ideally have liked to use chemical equilibrium calculations to predict the equation of state as a function of density, temperature and composition, either in-line during reactive flow simulations, or tabulated separately. In simulations of the type used here, the products generally pass through states which vary widely from the CJ isentrope, so it is important to choose the EOS carefully to ensure a stable calculation as well as for accuracy.

The Becker – Kistiakowski – Wilson (BKW) EOS [26] is unsuitable for this application as its structure, based on that of a perfect gas, is unphysical at high compression and low temperature. The Jacobs – Cowperthwaite – Zwisler (JCZ) family of EOS [27] are more suitable as the underlying formulation includes a $T = 0$ isotherm, but they were not available in the hydrocode in the necessary form in time for the calculations reported here. Instead, we used EOS developed for simulating mixed-species plasmas [30]. These EOS are based on arbitrary EOS for each pure specie, and can therefore be very accurate and physically correct for pure species at least.

There is some justification for this approach, other than computational expediency. Comparisons have been made between chemical equilibrium calculations using different computer programs, and mixture models [31]. It was found that state of the art chemical equilibrium calculations from different sources could predict equations of state which differed considerably. These equations of state were compared with the simpler mixed-species plasma models; equations of state derived from the mixture models lay between the chemical calculations, and tended to follow one or the other quite closely.

In essence, the plasma models mixed EOS for pure species without considering possible combinations of molecules through the free energy, and the EOS neglected or simplified cross-potentials between unlike species. Although there is no doubt that chemical equilibrium models with cross-potentials should be more accurate in principle than the mixture models, there was no real justification to choose one model over the other, and variants of the simple models were available in the hydrocode. The mixed-species EOS differed internally from those used previously [30] in that they were based around thermodynamically complete EOS for each pure species of the form $\{e,p\}(\rho,T)$ rather than $\{e,p\}(\rho,e)$. This modified form was computationally more efficient and less prone to numerical problems encountered when inverting tabular $\{e,p\}(\rho,T)$ EOS to obtain $\{e,p\}(\rho,e)$ EOS.

The other surprising observation was that the previous reasonable agreement with more rigorous equilibrium chemistry models for reaction products of CHNO-based propellants was achieved using a mixture of the EOS for C, H_2, N_2 and O_2 rather than more complicated molecules. In the present work, difficulties were encountered when water was included using any of the SESAME EOS, so the same prescription was used. We do not claim any fundamental justification for this model; it mainly reflects the difference between results from the different chemical equilibrium codes in this regime.

Given ρ, T for the mixture and the mass fraction f_i of the species, the contribution to e and p from each specie was deduced, using the temperature T of the mixture, and a value of the mass density ρ adjusted from the value for the mixture according to the mixing model used. Two such models were used: "partial density" and "constant number density". In the partial density model, the mass density was scaled by the mass fraction of that specie, so

$$\phi(\rho, T, f_i) = \sum_i \phi_i(f_i\rho, T) \tag{9}$$

where ϕ is the average quantity for the mixture (e, p or derivatives) and ϕ_i the corresponding expression for pure specie i. In the constant number density model, it is assumed for each specie in turn that all other molecules are of the same type, so

$$\phi(\rho, T, f_i) = \sum_i f_i\phi_i(\tilde{\rho}_i, T) \tag{10}$$

where

$$\tilde{\rho}_i = \rho m_i \sum_j f_j/m_j \tag{11}$$

and m_i is the molecular weight of specie i. This model is generally more accurate at high density.

9 Reaction rates

A generalized Arrhenius form was used for the chemical reaction rates:

$$\dot{\lambda} = R_0 \exp(-T/T^*) \tag{12}$$

T^* is the activation energy for reaction, and R_0 is the attempt frequency for effective collisions. T^* and R_0 may be functions of ρ and T, though in the present work constants were used. Further investigation of the coefficients in the rate might permit the model to reproduce steric hindrance and other physical phenomena that may limit the facility of a chemical reaction [40].

For a given shock input pressure, the temperature determined on the Hugoniot by the quasiharmonic method described above may not be accurate, because it is based on an equilibrium division of the added energy between vibrational modes of the molecule. Under shock loading, it may be anticipated that a non-equilibrium distribution of energy exists. It has been proposed [18] that low-frequency vibrations, those that couple well to the phonon modes of the solid, are most likely to be excited in shock-heating, and that higher lying vibrations are activated only slowly. However, as no examples of mode-specific excitation leading to reaction have yet been identified [39] we used the temperature defined by the equilibrated vibrations to govern the reactions of the molecule.

As discussed above, we included a surface burn contribution to the reaction rate. The Arrhenius rate was used to predict when significant surface burning would occur, and a flame propagation model was used in this situation. The flame speed would ideally be calibrated by mesoscale simulations of reaction with heat

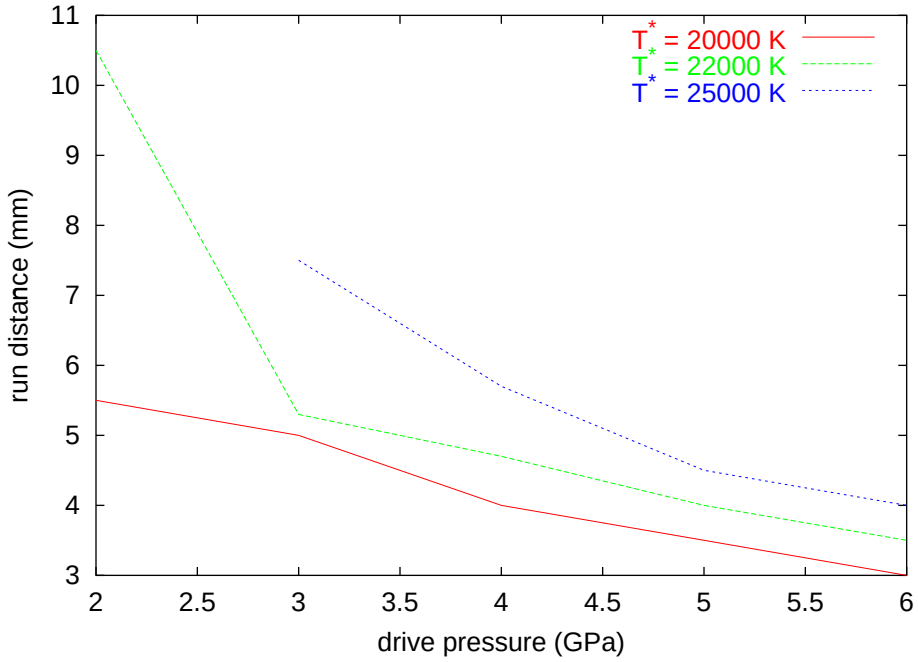

Figure 10: Sensitivity of run distance to T^*. Surface reactions, $\tau_p = 0.1\,\mu$s, $\tau_t = 1.0\,\mu$s, 45% porous, mesh size = 0.5 mm.

conduction; here we chose a constant value of the flame speed and investigated the sensitivity of different choices. The surface contribution requires an estimate to be made of the relation between the common surface area a_{ij} between each pair of components and the volume fraction of each. We estimated this relation using functional of the volume fraction of each:

$$a_{ij} \propto f_i^{2/3} f_j^{2/3}. \tag{13}$$

The constant of proportionality was obtained by using the grain size to estimate the number density of grains, and calculating their approximate surface area between two components of $f_i = f_j = 1/2$.

The energy release on reaction was determined from thermodynamic tables of the enthalpy of formation [23, 41].

9.1 Calibration for AN

Limited run distance data exist for porous AN, measured using electromagnetic particle velocity gauges [32] as discussed above. The run distance for AN of 45% porosity was observed to be ~4 to 5 mm when initiated at a particle speed of 1.18 km/s. The Arrhenius rate for AN alone was calibrated against this data.

The pressure applied to give the observed particle speed (1.18 km/s) was calculated using the unreactive porous model to be 3.0 GPa. The modal grain size was 250 μm [32], suggesting a time scale for pressure equilibration ~0.1 μs. The time scale for thermal equilibration was taken to be an order of magnitude larger. The modal grain size was also used to estimate the magnitude of the surface area contribution to the reaction rate.

As a starting point, the frequency factor Z was taken to be 10^{14}/s, which is a typical frequency of atomic vibration. The activation energy T^* was then adjusted by simulating shock initiation until the run distance was similar to the observed value (Fig. 10).

We found that a run distance of the correct order was given with $T^* \simeq 25000$ K for the surface burn model, and $T^* \simeq 20000$ K for bulk reaction only. Simulations were used to predict the run distance as a function of drive pressure and porosity (Fig. 11). The sensitivity to mesh size was found to be very close to linear (Fig. 12).

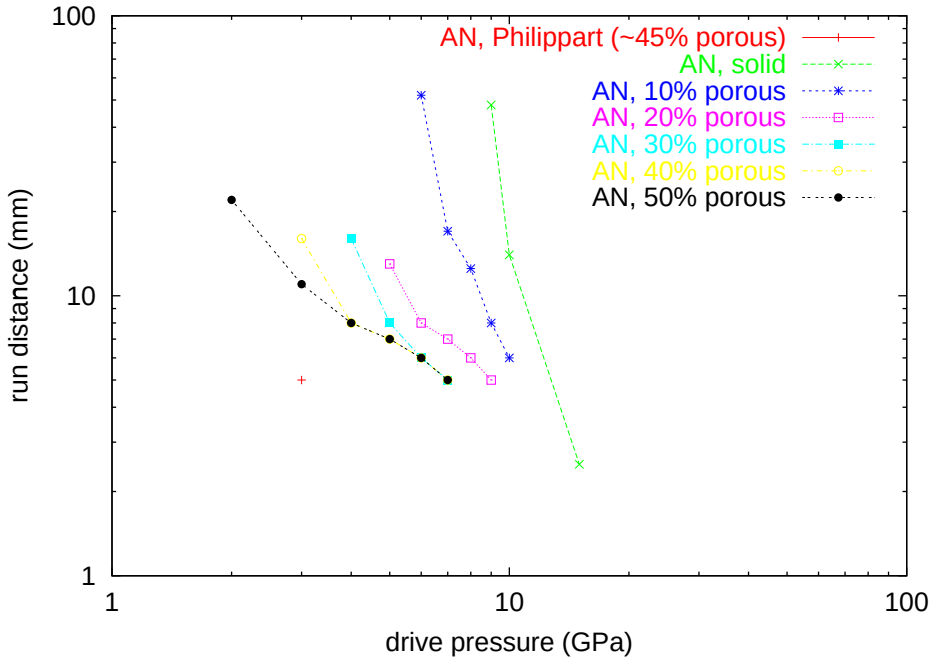

Figure 11: Pop plots for AN of different porosity. No surface reactions, $\tau_p = 0.1\,\mu$s, $\tau_t = 1.0\,\mu$s, mesh size = 1.0 mm.

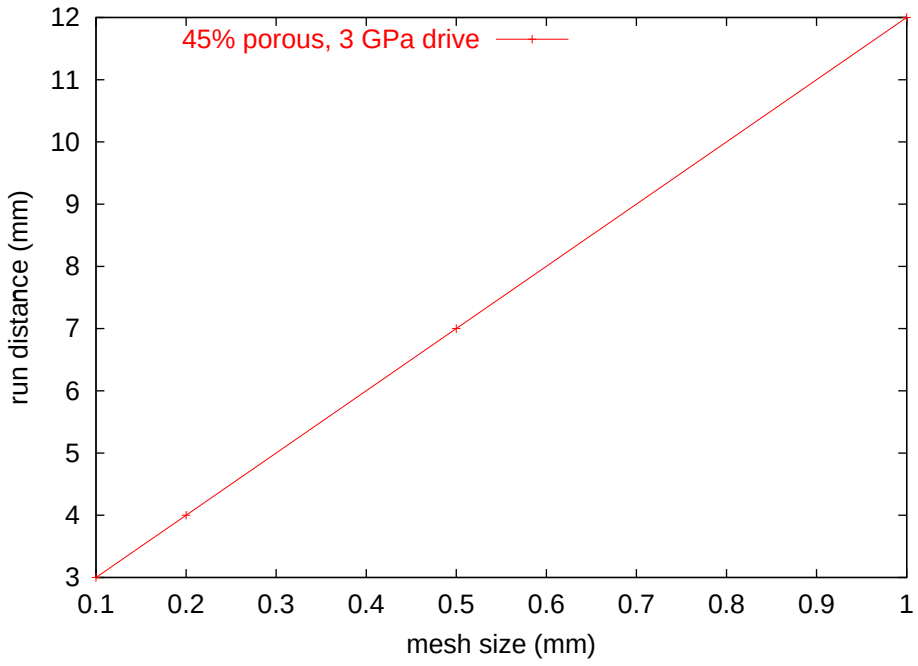

Figure 12: Mesh sensitivity of run distance in AN. No surface reactions, $\tau_p = 0.1\,\mu$s, $\tau_t = 1.0\,\mu$s.

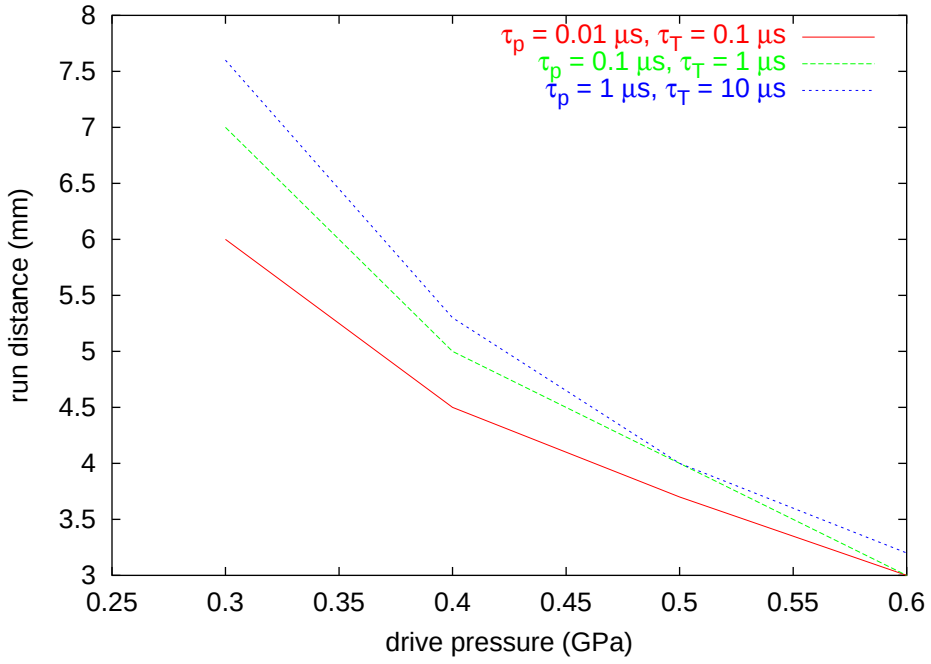

Figure 13: Sensitivity of AN run distance to time constants for equilibration. Porosity 45%, no surface reactions, drive pressure 3 GPa, mesh size = 0.5 mm.

The mesh dependence allows one to predict the mesh size required to obtain a converged simulation; in this case $\sim$ 0.01 mm for errors in run distance well below 10% (reasonable for simulations of initiation) at a drive pressure $\sim$3 GPa. It is also possible to provide a predictive capability with much coarser meshes if the relation between run distance and mesh size is known, by adjusting parameters in the rate law. The disadvantage in running without a converged system is that it may be necessary to adjust the parameters for different drive pressures, and this adjustment becomes more complicated if the applied loading does not give a constant pressure drive. We did not investigate the off-converged properties exhaustively in the present work, but off-converged mesh resolutions were used in most cases to reduce the computational time required.

Further simulations were performed to investigate the sensitivity to different parts of the model. The equilibration rates made a significant difference if changed by an order of magnitude (Fig. 13).

9.2 Calibration for ANFO

For the purposes of demonstration, calibration and comparison with ANFO was done using the formulation RX-HD, for which Lee-Tarver initiation parameters have been calculated [26]. Lee-Tarver simulations of shock initiation were used as run distance data, though this approach should be treated with caution since the Lee-Tarver parameters applied to overdriven detonation.

By mass, RX-HD contains 78.65% AN, 9.45% water, 5.52% calcium nitrate, 6.38% fuel oil, and 0.08% plastic microballoons. This composition is sufficiently complicated that mixing or EOS problems are likely to obscure effects from the reactive flow model, so a simplified composition was considered for the calibration. We took proportions by mass of 78.65 AN to 15.83 fuel oil, giving 83% and 17% respectively. In our reactive flow model the components are specified by volume; these mass proportions correspond to 72% and 28% respectively. The microballoons control the porosity, but the mass of the plastic wall makes it difficult to infer a porosity directly. We assumed that the difference between the mass density of the simplified mixture and that of RX-HD was accounted for by the porosity – a reasonable assumption – which gave a porosity $\sim$12%. The volume fractions of the condensed components were reduced proportionately, and the pore volume modelled as gas. As discussed above, the pore gas was taken to be AN decomposition products at

STP, though simulations were also performed using EOS for air to investigate any sensitivity. The initiation behaviour of the model was not sensitive to the EOS used for this initial pore gas.

The vaporisation of fuel oil was modelled by assigning an evaporation rate which was zero below the boiling temperature T_b and had a time scale of $1\,\mu$s to boil all the fuel above T_b. T_b was taken to be constant, though more rigorously it should increase with compression. Reaction of the vapour with oxygen in the product gases was modelled with an Arrhenius rate. The frequency factor was again taken to be 10^{14}/s, and the barrier temperature T^* was estimated roughly from the flash point of paraffin vapour. For computational efficiency, reaction in the products was neglected in most of the simulations of RX-HD, on the grounds that it would be unlikely to have as great an effect on the run distance for shock initiation as would the decomposition rate in the AN.

This simplified model of RX-HD was used in simulations of shock initiation with a drive pressure of 5 GPa. Ideally, we would hope for the simulations to agree with the 'data' – which was in this case another simulation based on an empirical model extrapolating outwith its probable range of validity. The predicted run distance was considerably greater than that predicted by the Lee-Tarver model. Without data on a simpler composition to compare against, we could not distinguish between inadequacies in the various parts of our model and in the Lee-Tarver model. It seems likely that part of the problem lies with the Lee-Tarver model, because the refinements neglected in our model would mostly give an even greater run distance: plastic flow is likely to decreased the run distance in pure AN, compared with RX-HD where the composition includes liquids, for a given Arrhenius model. The fact that the AN data included only a single shock initiation point is a possible source of error, but again this could imply an even smaller relative sensitivity of AN compared with RX-HD because the single point for AN lay among several of similar pressure where no shock initiation was observed. It is possible that reaction in the products should have been included in all the simulations of shock initiation. This will be investigated in future work.

To allow run distance trends to be compared with the Lee-Tarver model, the Arrhenius barrier temperature T^* for the decomposition of AN was adjusted to reproduce the Lee-Tarver prediction. Depending on mesh size, we found that an Arrhenius parameter $\sim$12000 to 15000 K was required. Based on our previous experience with HMX-based explosives, this adjustment is significant but falls within a range which can probably be addressed by making relatively minor improvements to the models.

10 Predicted shock sensitivity for RX-HD

The model for RX-HD was used to predict the variation of run distance with driving pressure. As discussed above, these predictions were compared with Lee-Tarver simulations intended to represent empirical data. The simulations used a mesh size of 0.5 mm. Run distances were obtained by inspection of graphs of the position – time history of the leading shock. These estimates were accurate to about 0.5 mm.

The initiation data from Lee-Tarver calculations were consistent with the present model using an Arrhenius barrier temperature T^* between about 12000 and 15000 K. This range was obtained by adjusting T^* to reproduce the run distance for a drive pressure of 5 GPa, but it is encouraging that the slope of the Pop plot matches the reference data reasonably well. (Fig. 14.)

11 Conclusions

A physically-based reactive flow model for ANFO explosives has been developed, based on our previous heterogeneous model for HMX-based explosives. The model uses thermodynamically complete equations of state and Arrhenius reaction rates with a surface burn term representing hotspots.

Condensed phase equations of state were predicted from shock wave data and estimates of the vibrational modes in each type of molecule. The resulting quasiharmonic equations of state were fairly consistent with the shock wave data, but could usefully be improved by adjusting the cold curve and using a more detailed treatment of the variation of vibrational frequencies with compression.

Porosity was modelled explicitly by including a volume fraction of gas in the virgin material. AN Hugoniots were predicted for porosities up to 50%, and compared with experimental data at 45%. The quasiharmonic EOS provided a reasonable fit to the data; an empirical EOS fitted to the shock wave data for solid AN gave excellent agreement with the porous data, suggesting that the quasiharmonic EOS should be

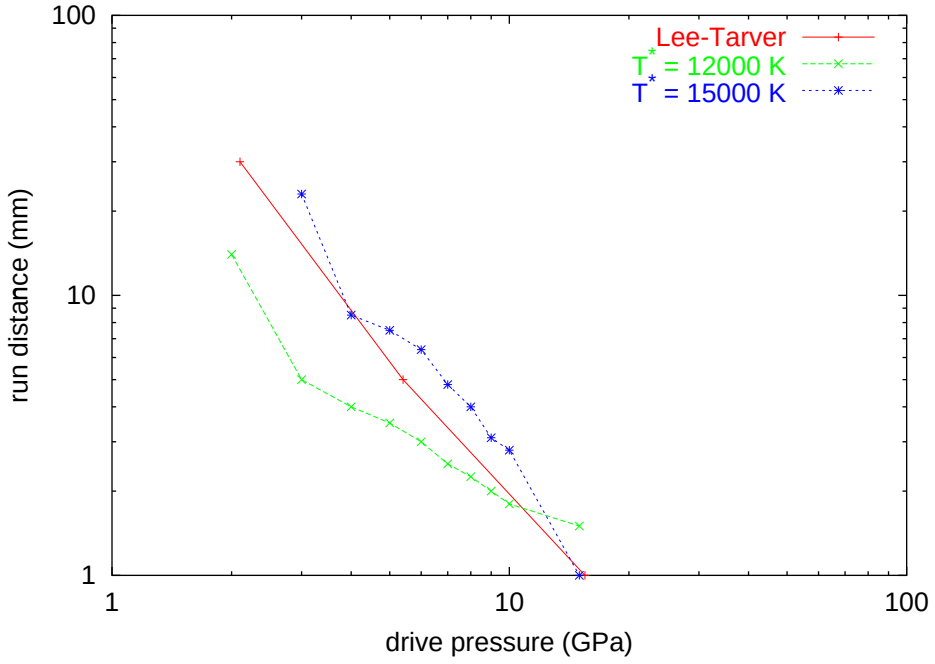

Figure 14: Pop plots for ANFO composition RX-HD.

adjusted slightly to improve its match to the solid Hugoniot. However, the porosity model itself appears to be perfectly adequate even at these rather large porosities, and it is recommended for continuum mechanics simulations.

The model can predict effect of composition, porosity, and particle size on the run to detonation as a function of loading conditions. Within the limitations of the sparse EOS and reaction data used for calibration, predictions made using the model are comparable with empirical data. The advantage of this model is that it allows initiation properties to be predicted from the properties of the components of a heterogeneous explosive, rather than requiring the behaviour to be measured for each new composition and morphology.

12 Future work

An important improvement to the model would be to include equilibrium chemistry for the equation of state of the reaction products. Off-Hugoniot data for AN would be helpful, from static press or dynamic loading experiments. It would also be extremely useful to include more initiation data in calibrating the reaction rates. This is always a problem for non-ideal explosives because very large charges may be required to achieve a 1D initiation. However, we would like to investigate an alternative strategy of using much higher drive pressures (multi-tens of GPa to a few hundred GPa), such as those available from lasers [42], to calibrate the reaction models in the limit of short run distance. Using large enough lasers, it should be possible to drive a well-supported shock into a representative sample of the energetic material. It should then be adequate to verify and adjust the model using a small number of comparisons with 2D data at low drive pressures.

We intend to use the model to simulate and interpret diameter effect data, and also to apply the model with different fuels. We plan eventually to include additional short-lived chemical species, allowing us to predict the effect of chemical desensitisers.

This model opens the door to the inclusion of chemical reaction data, in which behaviors are described as a function of temperature, in modelling of behaviors under shock loading.

Detailed kinetic observations may be used to guide the selection of Arrhenius constants, particularly R_0. Steric hindrance and other detailed mechanisms may be treated by manipulation of frequency term, or use of

multiple pathways with a high activation energies. Competitive multiple pathways may be included directly.

Incorporation of more complete kinetics by including intermediate chemical products is possible in principle, by increasing the number of dicrete chemical component in each cell. This level of detail is complicated by the dispersal of the intermediates on a timescale competitive with their reaction.

References

[1] D L Kennedy, *Multi-valued normal shock velocity versus curvature relationships for highly non-ideal explosives*, Proc 11th International Detonation Symposium, held Snowmass, Colorado, USA, 30 Aug to 4 Sep 1998, ONR 33300-5 (2000).

[2] R N Mulford and D C Swift, *Reactive flow models for the desensitisation of high explosives*, Proc. International Workshop on Non-Ideal Explosives, held Socorro, New Mexico, USA, Mar 1999, EMRTC (2000).

[3] R N Mulford and D C Swift, *Reactive flow models for the desensitisation of high explosive*, Proc APS Topical Conference on Shock Compression of Condensed Matter, held Snowbird, Utah, USA, Jun 1999, AIP (2000).

[4] D C Swift, unpublished work on thermodynamically complete equations of state for nitromethane (1998).

[5] G Wanstall (DERA Fort Halstead), private communication (2001).

[6] M Chaudhri and J E Field, Proc Roy Soc **A340**, 113 (1974).

[7] J R Waldram, "Introduction to thermodynamics," Cambridge (1984).

[8] N Whitworth and J Maw, *Modelling 'hot-spot' initiation in heterogeneous solid explosives*, Proc APS Topical Conference on Shock Compression of Condensed Matter, held Snowbird, Utah, USA, Jun 1999, AIP (2000).

[9] R N Mulford and D C Swift, *Mesoscale modelling of shock initiation in HMX-based explosives*, Proc APS Topical Conference on Shock Compression of Condensed Matter, held Atlanta, GA, 25 to 29 Jun 2001 (to appear).

[10] I. C. Skidmore, *An Introduction to Shock Waves in Solids*, Applied Materials Research pp 131 –147 (July 1965).

[11] D J Steinberg, *Equation of State and Strength Properties of Selected Materials*, Lawrence Livermore National Laboratory report UCRL-MA-106439 change 1 (1996).

[12] D C Swift, *Steinberg-Style Grüneisen Equations of State for Cerium, Lanthanum and Scandium*, Los Alamos National Laboratory report LA-UR-01-3005 (2001).

[13] S P Marsh (Ed), "LASL Shock Hugoniot Data", University of California (1980).

[14] Courchinoux and P Lalle, *Unreacted Hugoniot of ammonium nitrate,* High Pressure Science and Technology, 1993, published by the American Institute of Physics, Woodbury, NY, pp. 1397-1398.

[15] F Sandstrom, *Equation of state of ammonium nitrate and ammonium perchlorate,* MSc Thesis, EMRTC, New Mexico Tech., USA, Dec. 1994.

[16] M. van Thiel, *Compendium of Shock Wave Data*, Lawrence Radiation Laboratory report UCRL-50108 (1966).

[17] S. Lyon and J. D. Johnson (Los Alamos National Laboratory), private communications on 'SESAME' equation of state database (1998).

[18] D.D. Dlott and M.D. Fayer, J. Chem. Phys., 92, 3798, (1990).

[19] Kazuo Nakamoto, "Infrared and Raman Spectra of Inorganic and Coordination Compounds, 4th Edition." John Wiley and Sons, Inc. 1986.

[20] T. Shimanouchi, "Tables of Molecular Vibrational Frequencies, NSRDS NBS 39," Nat. Stand. Ref. Data Ser., Nat. Bur. Standards (U.S.), 39, 1972.

[21] T. Shimanouchi, "Tables of Molecular Vibrational Frequencies, Consolidated Volume II," Journal of Physical and Chemical Reference Data, 6(3), p. 993-1102 (1977).

[22] T. Shimanouchi, "Tables of Molecular Vibrational Frequencies, Part 9," Journal of Physical and Chemical Reference Data, 7(4), p. 1323-1443 (1978).

[23] G C Pimentel and R S Spratley, "Understanding Chemistry," Holden-Day, San Fransisco (1971).

[24] D.J. Steinberg,*Equation of state and strength properties of selected materials,* Lawrence Livermore National Laboratory report UCRL-MA-106439 (1996).

[25] J M Heimerl, Presented to the International Workshop on Non-Ideal Explosives, held Socorro, New Mexico, USA, Mar 1999, EMRTC (2000).

[26] P.C. Souers and L.C. Haselman Jr, *Detonation equation of state at LLNL,* Lawrence Livermore National Laboratory report UCRL-ID-116113 (1994).

[27] M Cowperthwaite and W H Zisler, *The JCZ equations of state for detonation products and their incorporation in the TIGER code*, Proc 6th Symposium (International) on Detonation, Office of Naval Research report ACR-221 (1976).

[28] K S Holian, *T-4 Handbook of Material Properties Data Bases, Vol. 1c: Equations of State*, Los Alamos National Laboratory report LA-10160-MS (1984).

[29] J M Winey, G E Duvall, M D Knudson and Y M Gupta, *Equation of state and temperature measurements for shocked nitromethane*, J Chem Phys vol. 113 no. 17 pp 7492 – 7501 (2000).

[30] D C Swift, *Hydrocode modelling of plasma capillaries*, presented to APS Division of Plasma Physics meeting, held New Orleans, Louisiana, USA, Nov 1998.

[31] D C Swift (Fluid Gravity Engineering Ltd), unpublished work on equations of state calculated using equilibrium chemistry codes (1999).

[32] D A Philippart and S G Hookings, *The unreacted Hugoniot of powdered ammonium nitrate,* in Proc. of the International Workshop on Non-Ideal Explosives, held Socorro, New Mexico, USA, Mar 1999, EMRTC (2000).

[33] N Asfanasenkov, V M Bogomlov and I M Voskoboinikov, *Generalized shock Hugoniot of condensed substances,* Zh. Pikl. Mekh. Fiz. 10, p. 660, 1970.

[34] Thouvenin, *Effect of a shock wave on a porous solid,* Proc. 4th Symposium. (Int.) on Detonation 1965, pp. 258-265, White Oak, Springfield, Maryland, USA; see also Meyers, *Dynamic behavior of materials,* John Wiley and Sons, 1994.

[35] D C Swift and R N Mulford, *A numerical scheme for reacting mixtures of materials in continuum mechanics simulations*, paper in preparation (2001).

[36] J R Ferraro, "Vibrational Spectroscopy at High External Pressures," Academic Press, Inc., Orlando, Florida, 1984.

[37] D. Philippart, *The study of booster materials with electromagnetic particle velocity gauges,* pp. 447-459, *8th Symposium (International) on Detonation, Albuquerque, New Mexico, USA, July 1985.*

[38] G. Wanstall, DERA, Fort Halstead. private communication regarding the uncontrolled nature of AN. Properties of AN vary with the degree of hydration and the grain size, and most measurements made do not report the characteristics of the measured samples of AN in sufficient detail to permit comparison between measurements.

[39] C B Moore and I W M Smith, *Chemical reactions of vibrationally excited molecules*, Faraday Discussions, Chem Soc **67** 196 (1979).

[40] K Yeager, talk on urea-nitric acid, this meeting.

[41] Langes Handbook of Chemistry, 44th Edition.

[42] D. L. Paisley, D. C. Swift, R. P. Johnson, R. A. Kopp and G. A. Kyrala, *Laser-launched flyer plates and direct laser shocks for dynamic material property measurements*, Proc APS Topical Conference on Shock Compression of Condensed Matter, held Atlanta, GA, 25 to 29 Jun 2001 (to appear).